A Global Optimization Framework for Joint Generation and Transmission Expansion Planning with AC Power Flow Representation

Ghazaleh Mozafari[a], Mahdi Mehrtash[b,c,*], Yankai Cao[a], Bhushan Gopaluni[a]

[a]*Department of Chemical and Biological Engineering, The University of British Columbia, Vancouver, BC, Canada, V6T 1Z3*
[b]*Department of Electrical and Biomedical Engineering, University of Nevada, Reno, NV 89557, USA*
[c]*Ralph O'Connor Sustainable Energy Institute, The Johns Hopkins University, Baltimore, MD 21218, USA*

Abstract

The integration of renewable energy generating units, often located in remote regions with limited grid connectivity, has created a pressing need for coordinated generation and transmission expansion planning (G&TEP). However, considering full AC network representation, the co-optimization of generation and transmission poses a challenging non-convex mixed-integer problem that is prone to locally suboptimal solutions. In this study, we propose a tailored global optimization framework to identify the most cost-effective set of generating units and candidate transmission lines while satisfying operational and investment constraints. The proposed solver employs second-order cone relaxation, further enhanced through a set of relaxation-tightening constraints, along with feasibility-based and optimization-based bound tightening techniques to improve relaxation strength. A salient feature of the solver is the integration of a no-good cut technique, which enables efficient exploration of alternative candidate solutions within the feasible region. As demonstrated by numerical results, this technique is specifically tailored to the G&TEP problem and significantly improves solution quality while reducing the runtime required to achieve global optimality. A comparative performance analysis with state-of-the-art global MINLP solvers demonstrates that the proposed approach achieves tighter optimality gaps more quickly and exhibits superior flexibility and scalability.

Keywords: Generation and transmission expansion planning, Global optimization, second-order cone programming, optimization-based bound tightening, no-good cuts

*Corresponding author. Email: mahdi.mehrtash@ieee.org

Nomenclature

Sets	
G/G^+	Existing/candidate generating units.
$\mathcal{L}/\mathcal{L}^+$	Existing/candidate lines.
G_n/G_n^+	Existing/candidate generating units at bus n.
D_n	Demands at bus n.
Indices	
g	Index for generating units.
n, k	Indices for buses.
l	Index for transmission lines.
x^R/x^S	Index for receiving/sending bus.
$t(l)/f(l)$	Receiving/sending terminal of line l.
x^0/x^1	Disaggregated variables of x in the hull formulation.
$\overline{x}/\underline{x}$	Upper/lower bound of x.
Parameters	
OC_g	Operation costs of unit g.
OC_n	Operation costs of the reactive compensator at bus n.
σ	Weight of the operation costs.
IC_l	Annualized investment cost for candidate line l.
IC_g	Annualized investment cost for unit g.
IB_l	Annualized investment budget for constructing new lines.
IB_g	Annualized investment budget for constructing new generating units.
V_n^{max}/V_n^{min}	Maximum/minimum voltage at bus n.
M	Big-M value.
B_l	Susceptance of line l in π-model.
G_l	Conductance of line l in π-model.
G_n^{sh}	Shunt conductance at bus n.
B_n^{sh}	Shunt susceptance at bus n.
$Q_{Cn}^{max}/Q_{Ln}^{max}$	Maximum reactive power generated/consumed by compensator located at bus n.

Continued on next page

C_l^{max}	Capacity of transmission line l.
P_g^{max}/P_g^{min}	Maximum/minimum active power capacity of generating unit g.
Q_g^{max}/Q_g^{min}	Maximum/minimum reactive power capacity of generating unit g.
RT	Setting for enabling relaxation-tightening constraints.
G	Flag for considering generation expansion programming.
np	Number of parallel computing threads.
Continuous variables	
V_n	Voltage at bus n.
θ_n	Voltage angle at bus n.
θ_l	Voltage angle difference across line l.
u_n	Auxiliary variable for voltage at bus n in conic model.
R_l/I_l	Auxiliary variables for line l in conic model.
P_g/Q_g	Active/reactive generation power at unit g.
P_l/Q_l	Active/reactive power flow through line l.
Q_{Cn}/Q_{Ln}	Reactive power generated/consumed by compensator at bus n.
SR_l/CR_l	Variables for sine/cosine relaxation of line l.
Integer variables	
x_l	Binary decision variable for candidate line l selection.
x_g	Binary decision variable for candidate generating unit g selection.

1. Introduction

Power system expansion planning is a long-term decision-making process that involves determining the optimal expansion and upgrading of power system components to meet future demand while ensuring the reliability and security of the electrical grid[1, 2]. A key component of this process is transmission expansion planning (TEP), which aims to decide on the location, number, and installation timing of new transmission lines to accommodate demand growth at the least total cost over a specified planning horizon.

Considering AC network representation, The TEP optimization problem is recognized as a NP-hard problem, non-linear and highly non-convex problem, posing significant challenges in achieving an optimal solution, especially for large systems[3].

To alleviate this complexity, the DC network representation has been extensively considered in TEP (i.e., DC-TEP) [4, 5, 6]. The DC network representation simplifies the problem by ignoring voltage stability, reactive power flows, and power losses, thereby allowing for linear models. For example, in [6], DC-TEP is modeled as a mixed-integer linear programming (MILP) model using disjunctive programming techniques. However, studies such as [7] have shown that a major drawback of DC models is that they often produce solutions that are infeasible when applied to AC network-based TEP (i.e., AC-TEP).

Consequently, many attempts have been made in the literature to solve the non-convex AC-TEP problem using convex relaxations. An approximation of the AC-TEP problem was proposed by [8] using the conic programming relaxation technique, which can significantly reduce computational complexity by convexifying the feasibility space. However, this approach may still yield infeasible solutions for the exact AC-TEP. Recently, a global optimization solver for AC-TEP problem was introduced in [9] utilizing a branch-and-bound algorithm based on semi-definite programming (SDP) relaxation. Although SDP models are widely regarded as the strongest relaxations for AC-TEP, they are computationally expensive specially for large systems. Moreover, as branch-and-bound must solve an SDP subproblem for a significant number of tree nodes, it lacks scalability. To address this limitation, [10] proposed an alternative advanced global solver for AC-TEP problem based on second-order cone programming (SOCP) relaxation, which is further incorporating relaxation-tightening constraints to improve the tightness of the relaxation. Compared to the SDP-based approach, this SOCP-based solver demonstrated superior scalability and significantly reduced runtimes.

Another key component of power expansion planning is generation expansion planning (GEP), driven by the need to meet increasing demand, aging infrastructures, and growing integration of renewable energy resources. GEP determines the optimal location and capacity of new generating units. It is typically approached in one of two ways: a market-based model, where private entities invest to optimize returns in competitive markets, or a centralized model, known as integrated resource planning (IRP), where a central authority plans and coordinates generation expansion to meet system reliability and policy goals. The centralized approach is explored in [11], which develops a multi-objective MILP (MOMILP) model for GEP. This model optimizes three objectives: minimizing expansion investment costs, reducing the environmental impact of installed capacity, and minimizing the environmental impact of energy generation.

Traditionally, GEP and TEP are planned independently, as they are managed by different market entities. However, the increasing penetration of renewable energy

resources into power systems makes it essential to jointly address GEP and TEP[12]. The optimal locations for renewable installations, such as areas with the best wind or solar conditions, are often far from demand centers and have poor interconnections with the transmission network [1]. This mismatch can lead to renewable energy curtailment due to limited transmission capacity and potential violations of voltage stability constraints. A comparative study in [13] demonstrated that co-optimizing generation and transmission expansion planning (G&TEP) achieves significant cost reductions compared to solving GEP and TEP problems separately. This improvement arises from the strong interdependencies between TEP and GEP, which render separate planning approaches suboptimal.

In recent years, researchers have increasingly focused on co-optimizing the G&TEP problem. Several studies have concentrated on DC network representation (i.e., DC-G&TEP) [14, 15, 16, 17]. For instance, [17] developed and compared three different MILP formulations for DC-G&TEP utilizing Benders decomposition algorithm. While DC-based expansion planning models offer computational efficiency, they fail to accurately represent voltage stability, reactive power constraints, and nonlinear AC power flow, and may be infeasible in for AC network-based plannings. Furthermore, a comparative study reveals significant differences in the solutions of DC and AC based planning, highlighting the necessity of considering AC network representation for more accurate and feasible planning solutions [18].

The AC-based coordinated G&TEP (i.e., AC-G&TEP) has also been explored using convex relaxations of AC power flow models [19, 20]. Specifically, [19] employed linearized AC power flow models using first-order Taylor series approximations. However, these relaxations may produce infeasible solutions for the exact AC model. Additionally, the non-convex AC-G&TEP problems have also been addressed locally using heuristic methods such as genetic algorithms [21] and metaheuristic methods [22, 23]. For instance, in [24] using generic algorithms first find the binary variables related to generating units and transmission lines, and then substituting the obtained solution, solve the NLP problem locally. While these approaches can yield feasible solutions, they can not guarantee convergence, and they often converge to local optima, which may be significantly far from the global optimum. Determining the deviation of these local optima from the global optimum is not trivial. For large-scale economic assessments, such as power system planning that spans 15 to 20 years as a planning horizon and does not require real-time solutions, aiming for a guaranteed global optimum is preferable.

Despite recent advances in global optimization methods for AC-TEP, there remains a significant gap in the literature for frameworks that address G&TEP globally. Most existing approaches either rely on simplified linear or relaxed models that may lead to

AC infeasible solutions, or fail to provide convergence guarantees due to the inherent nonconvexity of the exact AC power flow equations. Furthermore, state-of-the-art general-purpose global solvers such as SCIP and Couenne struggle to handle the mixed-integer, highly non-convex structure of AC-G&TEP, particularly when applied to large-scale power systems.

Moreover, most existing methods for solving the G&TEP problem lack numerical validation on large-scale test systems. For example, the G&TEP model proposed in [22] is tested on 6-bus and 118-bus test systems, while the largest test system in [19, 25] is limited to 24 buses. However, these test systems might be insufficient to thoroughly assess the practicality of solution methods for real-world power systems. Therefore, validation on larger test systems is crucial to evaluate the scalability and effectiveness of the proposed approaches for practical implementation.

Motivated by the success of SOCP-based global solver in AC-TEP, the growing need for coordinated G&TEP, and the computational limitations of standard MINLP solvers in this domain, this work proposes a global optimization framework for co-optimizing the AC-G&TEP problem with guaranteed optimality gap. The proposed framework extends the Global-TEP model introduced in [10] by incorporating generation expansion and reactive power compensation planning, thereby enabling a more comprehensive long-term planning formulation. To the best of our knowledge, this is the first global optimization framework for solving the AC-based joint G&TEP problem with a guaranteed optimality gap. The main contributions of this paper are as follows:

- Two bound-tightening techniques are implemented to further improve the relaxation and refine the search space. Feasibility-based bound tightening (FBBT) is applied to narrow the bounds of decision variables for both existing and candidate lines in a noticeably short runtime. A novel optimization-based bound tightening (OBBT) method is introduced based on the continuous SOCP relaxation of the problem. The proposed OBBT is applied to both continuous variables and binary decision variables associated with candidate lines and generating units, potentially decreasing the number of binary variables in the problem and leading to a shorter solution time.

- A notable advancement in this study is the novel application of the no-good cut technique. By excluding previously obtained solutions using no-good cuts, the algorithm efficiently explores alternative candidate solutions within the feasible region. Numerical results indicate that this technique substantially reduces the computational runtime required to achieve the desired optimality gap.

- The performance of the proposed approach is compared with existing global MINLP solvers SCIP and Couenne. Numerical results illustrate that the proposed solver can reach high-quality solutions much faster. The AC-TEP version of the proposed approach is also compared with the most recent and advanced global AC-TEP solvers, demonstrating that the proposed approach outperforms them in terms of both solution quality and computational time.
- A large-scale 1354-bus test case is utilized to assess the scalability of the proposed method. The results demonstrate that the method can deliver high-quality solutions for such a large-scale MINLP problem within a reasonable runtime.

The remainder of this paper is organized as follows. Section 2 presents the mathematical formulation. The algorithm for the proposed approach (Global-G&TEP) is detailed in Section 3. Numerical results and discussions are provided in Section 4. Finally, Section 5 draws relevant conclusions.

2. Mathematical formulation

This section presents the AC-G&TEP formulation, which aims to determine the most cost-effective combination of candidate generating units and transmission lines to meet future demand and system constraints over a planning horizon, which is assumed to be 20 years in this study. The proposed Global-G&TEP framework is based on static network representation and formulated under the assumption of deterministic demand and generation profiles. The model also assumes centralized system planning, with the objective of minimizing the total annualized cost of generation and transmission infrastructure over the planning horizon. Additionally, the model incorporates the option to install reactive power compensators, which can reduce the need for costly line upgrades or new installations. The overall objective function, given in equation (1), includes investment costs associated with new generating units and transmission lines, as well as the operational costs of generation and reactive compensation. Operational costs are assumed to be linear with respect to generation output and are scaled by a weighting factor (denoted by σ) to ensure consistency with annualized investment costs, as in [26].

$$\min_{\Gamma} \sum_{g \in G^{+}} IC_g \cdot x_g + \sum_{l \in \mathcal{L}^{+}} IC_l \cdot x_l + \sigma \left(\sum_{g \in G} OC_g \cdot P_g + \sum_{n \in B} OC_n \cdot (Q_{Cn} + Q_{Ln}) \right) \quad (1)$$

The decision variables are presented in (2), including the binary variables for the installation of new lines and generating units, as defined in (3). If a candidate line

or generating unit is selected for construction, the associated binary variable is set to 1; otherwise, it is set to 0. Constraints (4) and (5) model the investment budget limitations for expansion planning over the planning horizon.

$$\Gamma = \{x_l, x_g, P_g, Q_g, P_l, Q_l, u_n, R_l, I_l, Q_{Cn}, Q_{Ln}\} \tag{2}$$

$$x_g, x_l = \{0, 1\}; \quad \forall g \in G^+, \forall l \in \mathcal{L}^+ \tag{3}$$

$$\sum_{g \in G^+} IC_g \cdot x_g \leq IB_g \tag{4}$$

$$\sum_{l \in \mathcal{L}^+} IC_l \cdot x_l \leq IB_l \tag{5}$$

Nodal balances for active and reactive power in the network are modeled in (6) and (7), respectively. Equations (8) through (11) model the active and reactive power flows for existing lines. The parameters G_l and B_l in these equations are calculated using the π-model representation of transmission lines [22]. For candidate lines, a disjunction can be used to express the relationship between the candidate line being installed and the corresponding power flow. According to the disjunctive constraints (12)-(15), if a candidate line is selected, the power flow through that line should satisfy the AC power flow constraints and bounds; otherwise, the power flow through that line should be zero. These constraints, initially nonlinear and non-convex, are further reformulated as a set of linear constraints in following section by applying disjunctive programming techniques. Constraints (16) and (17) set limits on the power flow through existing and candidate lines based on their transmission capacities. For system security, it is essential to keep the nodal voltage magnitude near a nominal value of 1.0 pu [27]. Constraint (18) ensures that the voltage at each bus remains within acceptable deviation limits from this nominal value, typically around 5%.

$$-\sum_{g \in G_n} P_g - \sum_{g \in G_n^+} P_g + \sum_{l|f(l)=n} P_l^S + \sum_{l|t(l)=n} P_l^R + \sum_{d \in D_n} P_d + G_n^{sh} u_n = 0; \forall n \tag{6}$$

$$-\sum_{g \in G_n} Q_g - \sum_{g \in G_n^+} Q_g + \sum_{l|f(l)=n} Q_l^S + \sum_{l|t(l)=n} Q_l^R + \sum_{d \in D_n} Q_d - B_n^{sh} u_n - Q_{Cn} + Q_{Ln} = 0; \forall n \tag{7}$$

$$P_l^S = G_l u_n - G_l R_l + B_l I_l; \quad \forall l \in \mathcal{L}, n = f(l) \tag{8}$$

$$P_l^R = G_l u_k - G_l R_l - B_l I_l; \quad \forall l \in \mathcal{L}, k = t(l) \tag{9}$$

$$Q_l^S = -B_l u_n + B_l R_l - G_l I_l; \quad \forall l \in \mathcal{L}, n = f(l) \tag{10}$$

$$Q_l^R = -B_l u_k + B_l R_l + G_l I_l; \quad \forall l \in \mathcal{L}, k = t(l) \tag{11}$$

$$P_l^S = (G_l u_n - G_l R_l + B_l I_l) \cdot x_l; \quad \forall l \in \mathcal{L}^+, n = f(l) \tag{12}$$

$$P_l^R = (G_l u_k - G_l R_l - B_l I_l) \cdot x_l; \quad \forall l \in \mathcal{L}^+, k = t(l) \tag{13}$$

$$Q_l^S = (-B_l u_n + B_l R_l - G_l I_l) \cdot x_l; \quad \forall l \in \mathcal{L}^+, n = f(l) \tag{14}$$

$$Q_l^R = (-B_l u_k + B_l R_l + G_l I_l) \cdot x_l; \quad \forall l \in \mathcal{L}^+, k = t(l) \tag{15}$$

$$(P_l^S)^2 + (Q_l^S)^2 \leq (C_l^{max})^2; \quad \forall l \in \{\mathcal{L}, \mathcal{L}^+\} \tag{16}$$

$$(P_l^R)^2 + (Q_l^R)^2 \leq (C_l^{max})^2; \quad \forall l \in \{\mathcal{L}, \mathcal{L}^+\} \tag{17}$$

$$(V_n^{min})^2 \leq u_n \leq (V_n^{max})^2; \quad \forall n \tag{18}$$

On the generation side, the active power generation limits for both existing and candidate units are constrained by their respective capacities, as defined in equations (19) and (20). Similarly, constraints (21) and (22) specify the bounds for reactive power generation. Additionally, constraints (23) and (24) model the reactive power limits of compensators.

$$P_g^{min} \leq P_g \leq P_g^{max}; \quad \forall g \in G \tag{19}$$

$$P_g^{min} x_g \leq P_g \leq x_g P_g^{max}; \quad \forall g \in G^+ \tag{20}$$

$$Q_g^{min} \leq Q_g \leq Q_g^{max}; \quad \forall g \in G \tag{21}$$

$$Q_g^{min} x_g \leq Q_g \leq x_g Q_g^{max}; \quad \forall g \in G^+ \tag{22}$$

$$0 \leq Q_{Cn} \leq Q_{Cn}^{max}; \quad \forall n \tag{23}$$

$$0 \leq Q_{Ln} \leq Q_{Ln}^{max}; \quad \forall n \tag{24}$$

In this study, we employ the polar power-voltage formulation of the AC optimal power flow (AC-OPF) problem. The relationships of u_l, R_l, and I_l are linked to the magnitude and angle of the nodal voltages through equations (25)–(27), which are non-convex and nonlinear. Although the variables u_l, R_l, and I_l are not necessary to

formulate the problem, they serve as auxiliary conic variables to facilitate a better understanding of the mixed-integer SOCP (MISOCP) relaxation of the problem.

$$u_n = (V_n)^2; \quad \forall n \tag{25}$$

$$R_l = V_n V_k \cos\theta_l; \quad \forall l \in \{\mathcal{L}, \mathcal{L}^+\}, n = f(l), k = t(l) \tag{26}$$

$$I_l = V_n V_k \sin\theta_l; \quad \forall l \in \{\mathcal{L}, \mathcal{L}^+\}, n = f(l), k = t(l) \tag{27}$$

2.1. Reformulation of disjunctive constraints

2.1.1. Big-M reformulation

The big-M reformulation is employed to model the disjunctive constraints as a set of linear constraints that describe the same feasible set by introducing a large positive value (i.e., M). Equations (28)–(35) represent the power flow constraints for candidate lines using the big-M technique. The selection of the M value significantly affects the feasible region and, consequently, the runtime. While the M value for each constraint needs to be sufficiently large, it should also be as small as possible to tighten the feasible region. To determine the smallest possible value of M for each constraint, we follow the instructions provided in [10]. For constraint (28), the smallest valid value of the M parameter is equal to the largest possible value of $\left|P_l^S - (G_l u_n - G_l R_l + B_l I_l)\right|$. Accordingly, M is defined as $\max\left\{\max\left[P_l^S - (G_l u_n - G_l R_l + B_l I_l)\right], -\min\left[P_l^S - (G_l u_n - G_l R_l + B_l I_l)\right]\right\}$. Assuming all parameters G_l and B_l are positive, and using the variable bounds $P_l^S \in [-C_l^{\max}, C_l^{\max}]$ (from (16)) and $u_n \in [(V_n^{\max})^2, (V_n^{\max})^2]$, the smallest valid M value simplifies to $M = C_l^{\max} + (B_l + G_l)(V_n^{\max})^2$. A similar interval-based arithmetic procedure is applied to determine the smallest valid values of M for constraints (30), (32), and (34).

$$|P_l^S - (G_l u_n - G_l R_l + B_l I_l)| \leq (1 - x_l) \cdot M; \quad \forall l \in \mathcal{L}^+, \, n = f(l) \tag{28}$$

$$|P_l^S| \leq C_l^{\max} \cdot x_l; \quad \forall l \in \mathcal{L}^+ \tag{29}$$

$$|P_l^R - (G_l u_k - G_l R_l - B_l I_l)| \leq (1 - x_l) \cdot M; \quad \forall l \in \mathcal{L}^+, \, k = t(l) \tag{30}$$

$$|P_l^R| \leq C_l^{\max} \cdot x_l; \quad \forall l \in \mathcal{L}^+ \tag{31}$$

$$|Q_l^S - (-B_l u_n + B_l R_l - G_l I_l)| \leq (1 - x_l) \cdot M; \quad \forall l \in \mathcal{L}^+, \, n = f(l) \tag{32}$$

$$|Q_l^S| \leq C_l^{\max} \cdot x_l; \quad \forall l \in \mathcal{L}^+ \tag{33}$$

$$|Q_l^R - (-B_l u_k + B_l R_l + G_l I_l)| \leq (1 - x_l) \cdot M; \quad \forall l \in \mathcal{L}^+,\, k = t(l) \tag{34}$$

$$|Q_l^R| \leq C_l^{\max} \cdot x_l; \quad \forall l \in \mathcal{L}^+ \tag{35}$$

2.1.2. Hull reformulation

Hull reformulation is a disjunctive programming technique used to convert a disjunctive constraint into a set of linear constraints by introducing disaggregated variables for each condition. These variables separate the conditions into distinct terms, with the summation of all disaggregated variables equaling the value of the original variable [28]. For example, in (36), u_n is split into u_n^0 and u_n^1, where u_n^1 represents the voltage when the line l is installed, and u_n^0 represents the voltage when it is not installed. Equations (36)–(51) represent the set of linear constraints obtained by reformulating the disjunctions (12)–(15) using hull reformulation. While this method increases the problem size by introducing additional continuous variables and constraints, it eliminates the need for big-M parameters.

$$u_n = u_n^0 + u_n^1; \quad \forall l \in \mathcal{L}^+, n = f(l) \tag{36}$$

$$u_k = u_k^0 + u_k^1; \quad \forall l \in \mathcal{L}^+, k = t(l) \tag{37}$$

$$R_l = R_l^0 + R_l^1; \quad \forall l \in \mathcal{L}^+ \tag{38}$$

$$I_l = I_l^0 + I_l^1; \quad \forall l \in \mathcal{L}^+ \tag{39}$$

$$\underline{u}_n \cdot (1 - x_l) \leq u_n^0 \leq (1 - x_l) \cdot \overline{u}_n; \quad \forall l \in \mathcal{L}^+, n = f(l) \tag{40}$$

$$\underline{u}_k \cdot (1 - x_l) \leq u_k^0 \leq (1 - x_l) \cdot \overline{u}_k; \quad \forall l \in \mathcal{L}^+, k = t(l) \tag{41}$$

$$\underline{R}_l \cdot (1 - x_l) \leq R_l^0 \leq (1 - x_l) \cdot \overline{R}_l; \quad \forall l \in \mathcal{L}^+ \tag{42}$$

$$\underline{I}_l \cdot (1 - x_l) \leq I_l^0 \leq (1 - x_l) \cdot \overline{I}_l; \quad \forall l \in \mathcal{L}^+ \tag{43}$$

$$\underline{u}_n \cdot x_l \leq u_n^1 \leq x_l \cdot \overline{u}_n; \quad \forall l \in \mathcal{L}^+, n = f(l) \tag{44}$$

$$\underline{u}_k \cdot x_l \leq u_k^1 \leq x_l \cdot \overline{u}_k; \quad \forall l \in \mathcal{L}^+, k = t(l) \tag{45}$$

$$\underline{R}_l \cdot x_l \leq R_l^1 \leq x_l \cdot \overline{R}_l; \quad \forall l \in \mathcal{L}^+ \tag{46}$$

$$\underline{I}_l \cdot x_l \leq I_l^1 \leq x_l \cdot \overline{I}_l; \quad \forall l \in \mathcal{L}^+ \tag{47}$$

$$P_l^S = G_l u_n^1 - G_l R_l^1 + B_l I_l^1;\ \forall l \in \mathcal{L}^+, n = f(l) \tag{48}$$

$$P_l^R = G_l u_k^1 - G_l R_l^1 - B_l I_l^1;\ \forall l \in \mathcal{L}^+, k = t(l) \tag{49}$$

$$Q_l^S = -B_l u_n^1 + B_l R_l^1 - G_l I_l^1;\ \forall l \in \mathcal{L}^+, n = f(l) \tag{50}$$

$$Q_l^R = -B_l u_k^1 + B_l R_l^1 + G_l I_l^1;\ \forall l \in \mathcal{L}^+, k = t(l) \tag{51}$$

In this work, we applied the big-M reformulation for the lower bounding (LB) problem presented later in the paper. This choice avoids increasing the problem size by introducing additional variables and constraints, as required by hull reformulation. However, for the continuous relaxed version of the problem, the hull reformulation technique is employed to achieve tighter relaxations, as suggested in [29]. The continuous relaxed problem is further utilized in OBBT process.

2.2. MISOCP relaxations of the AC-G&TEP

By introducing conic variables and reformulating the disjunctive constraints, equations (25)–(27) remain as the only non-linear and non-convex constraints. The MISOCP relaxation of AC-G&TEP is achieved by relaxing these constraints with a second-order cone constraint (52) for both existing and candidate lines. Therefore, key equations (1)-(11), (16)-(24), (28)-(35), and the constraint (52) define the MISOCP relaxation of the AC-G&TEP problem. This proposed MISOCP relaxation is convex and can be solved globally using standard MILP solvers such as CPLEX.

$$u_n u_k \geq (R_l)^2 + (I_l)^2; \quad \forall l \in \{\mathcal{L}, \mathcal{L}^+\}, n = f(l), k = t(l) \tag{52}$$

2.3. Relaxation-tightening constraints

To further tighten the MISOCP relaxed problem, several convex relaxation-tightening constraints are considered. Nodal voltage angle and magnitude are bounded as specified in equation (53). The angle difference over each line (i.e., θ_l) is defined and bounded in equations (55) and (56), respectively. Additionally, constraint 54 sets the voltage angle of the reference bus to zero. The next step involves relaxing the trigonometric terms of the constraints (26) and (27). A quadratic relaxation based on exploiting convex envelopes for cosine and sine terms is presented in (57)–(60) for both existing and candidate lines. These constraints are valid within the range $[-\pi/2, \pi/2]$. In this study, the maximum input angle difference is considered to be $\frac{\pi}{3}$. However, after applying FBBT and OBBT, this angle difference decreases significantly. Notably, in practical power network design, the acceptable phase angle difference can be as small as $\frac{\pi}{36}$, as reported in [29]. The

maximum possible estimation error of these relaxations is expressed in terms of θ_l [29]. As a result, tightening the bounds on angle differences significantly impacts the tightness of sine and cosine relaxations.

$$V_n^{min} \leq V_n \leq V_n^{max} \quad , \quad \underline{\theta}_n \leq \theta_n \leq \overline{\theta}_n; \qquad \forall n \tag{53}$$

$$\theta_{ref} = 0; \tag{54}$$

$$\theta_l = \theta_n - \theta_k; \quad \forall l \in \{\mathcal{L}, \mathcal{L}^+\}, n = f(l), k = t(l) \tag{55}$$

$$\underline{\theta}_l \leq \theta_l \leq \overline{\theta}_l; \quad \forall l \in \{\mathcal{L}, \mathcal{L}^+\} \tag{56}$$

$$CR_l \leq 1 - \frac{1 - \cos \overline{\theta}_l}{(\overline{\theta}_l)^2} \theta_l^2; \quad \forall l \in \{\mathcal{L}, \mathcal{L}^+\} \tag{57}$$

$$CR_l \geq \cos(\overline{\theta}_l); \quad \forall l \in \{\mathcal{L}, \mathcal{L}^+\} \tag{58}$$

$$SR_l \leq \cos(\frac{\overline{\theta}_l}{2}) \cdot (\theta_l - \frac{\overline{\theta}_l}{2}) + \sin(\frac{\overline{\theta}_l}{2}); \quad \forall l \in \{\mathcal{L}, \mathcal{L}^+\} \tag{59}$$

$$SR_l \geq \cos(\frac{\overline{\theta}_l}{2}) \cdot (\theta_l + \frac{\overline{\theta}_l}{2}) - \sin(\frac{\overline{\theta}_l}{2}); \quad \forall l \in \{\mathcal{L}, \mathcal{L}^+\} \tag{60}$$

Next, the convex hull of the trilinear terms in (26) and (27) is derived using the lambda technique, with the associated constraints detailed in [10]. Additionally, convex hull for the tangent function and a strong relaxation for the cycle basis constraint are also considered. A comprehensive description of these tightening constraints is provided in [10].

3. Solution algorithm

3.1. Bound tightening techniques

3.1.1. FBBT

FBBT is an effective bound tightening technique for tightening variable bounds with minimal runtime. It leverages interval arithmetic on problem constraints to determine feasible variable bounds [30], resulting in significantly tighter feasible region that improve solution times. Furthermore, since the tightness of relaxations depends on variable bounds, applying FBBT enhances the overall relaxation quality[30].

To demonstrate FBBT formulation, we present two examples of bound tightening using this approach. Based on equations (16) and (17), we can conclude that $\left\{P_l^S, P_l^R, Q_l^S, Q_l^R\right\} \in [-C_l^{\max}, C_l^{\max}]$. Applying interval arithmetic to the constraints

(8)–(11), we can calculate the feasible bounds for the variable I_l as (61) and (62). The same approach is applied to the variables R_l and u_n. To account for any numerical errors due to the computation process, a very small positive value ϵ (e.g., 10^{-10}) is considered. Subsequently, using the updated tightened bounds of these variables and considering equation (27), we can reduce the domain of θ_l as (63). FBBT is applied to other variables for both existing and candidate lines. Further details can be found in [10].

$$\begin{aligned}\underline{I}_l = \max\big\{\underline{I}_l, &\frac{G_l(V_n^{max})^2 - G_l\underline{R}_l + C_l^{max}}{-B_l} - \epsilon,\\ &\frac{G_l(V_n^{min})^2 - G_l\overline{R}_l - C_l^{max}}{B_l} - \epsilon,\\ &\frac{-B_l(V_n^{min})^2 + B_l\overline{R}_l + C_l^{max}}{-G_l} - \epsilon,\\ &\frac{-B_l(V_n^{max})^2 + B_l\underline{R}_l - C_l^{max}}{G_l} - \epsilon\big\}\end{aligned} \tag{61}$$

$$\begin{aligned}\overline{I}_l = \min\big\{\overline{I}_l, &\frac{G_l(V_n^{min})^2 - G_l\overline{R}_l - C_l^{max}}{-B_l} + \epsilon,\\ &\frac{G_l(V_n^{max})^2 - G_l\underline{R}_l + C_l^{max}}{B_l} + \epsilon,\\ &\frac{-B_l(V_n^{max})^2 + B_l\underline{R}_l - C_l^{max}}{-G_l} + \epsilon,\\ &\frac{-B_l(V_n^{min})^2 + B_l\overline{R}_l + C_l^{max}}{G_l} + \epsilon\big\}\end{aligned} \tag{62}$$

$$\underline{\theta}_l = \max\big\{\underline{\theta}_l, \arcsin\big(\max(\frac{\underline{I}_l}{V_n^{min}V_k^{min}}, \frac{\underline{I}_l}{V_n^{max}V_k^{max}})\big) - \epsilon\big\} \tag{63}$$

3.1.2. Proposed OBBT

The OBBT technique is widely used in MINLP problems to reduce the problem domain. It involves calculating the minimum and maximum values of a decision variable by solving a relaxed version of the problem. OBBT is based on the principle that the feasible region of the relaxed version of the problem encompasses that of the original problem; thus, the calculated minimum and maximum values serve as valid bounds for the corresponding variable. OBBT requires solving up to two optimization

problems for each variable, which can be computationally expensive, especially for large systems. However, because these optimization problems are independent, they can be solved in parallel.

To reduce the runtime of OBBT, we employ a continuous relaxed version of the problem by converting the integer variables to continuous variables in the range of $[0, 1]$. We utilize the hull reformulation technique for the power flow disjunctive constraints for candidate lines, as it is demonstrated in the literature that the hull reformulation technique leads to stronger continuous relaxations compared to the big-M technique [15, 29]. The continuous relaxed problem is an SOCP relaxation of the AC-G&TEP problem, which can be efficiently solved by existing solvers in a short runtime. Fig. 1 presents the performance of the proposed OBBT on θ_l for the IEEE 118-bus system, demonstrating that OBBT can significantly improve the bounds of θ_l for all existing lines, tightening them from the initial range of $[-\pi/3, \pi/3]$ to much narrower bounds, as shown by the green bars.

In this work, the OBBT technique is also applied to integer variables. If the maximum value of an integer variable obtained through OBBT is less than 1, the associated candidate line or generating unit is deemed infeasible and removed from the candidate set. This approach helps reduce the number of binary variables in the problem by eliminating infeasible candidates, thereby decreasing runtime. To the best of the authors' knowledge, this is the first application of OBBT to integer variables in G&TEP.

3.2. Lower/upper bounding problem

The proposed MISOCP relaxation serves as the LB problem for the AC-G&TEP problem. The proposed approach introduces a trade-off between the tightness of relaxation and computational complexity, controlled by the RT setting. When $RT = 0$, the nonlinear constraints of (25)–(27) are relaxed using constraint (52). By setting $RT = 1$ and $RT = 2$, the MISOCP relaxation is progressively tightened by incorporating relaxation-tightening constraints for existing transmission lines and extending these constraints to candidate lines, respectively. As a result, the RT setting makes the proposed approach more flexible.

For the upper bounding (UB) problem, the corresponding AC-OPF is solved by fixing the binary decision variables to the values obtained from solving the LB problem. Regardless of the fixed binary configuration, the resulting AC-OPF solution represents a locally optimal solution for the original AC-G&TEP problem and therefore provides a valid upper bound. It is important to note that, since the final power flow solution is derived from the AC-OPF, it remains fully AC feasible irrespective of the computed optimality gap.

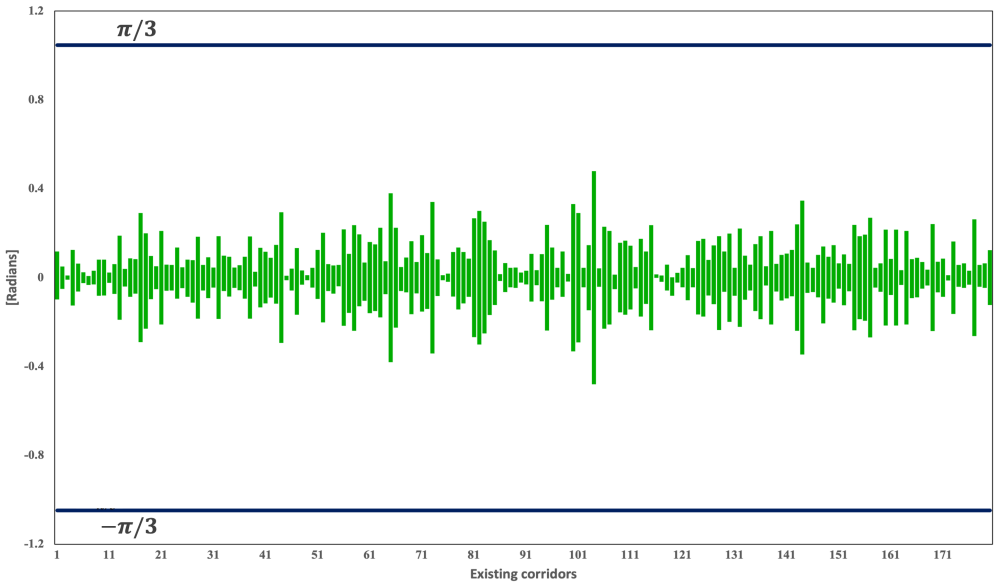

Figure 1: OBBT results on θ_l of existing lines for the IEEE 118-bus system.

3.3. No-good cuts

No-good cuts are constraints introduced during the solution process to exclude specific regions of the solution space, thereby preventing the solver from revisiting these areas. This approach is particularly beneficial in branch-and-bound algorithms, where it helps to prune the search tree, excluding regions associated with suboptimal solutions, and reducing computational burden [31]. One general form of this constraint is given in (64) that excludes a particular solution $\hat{x}$ of a problem region. By choosing a proper ϵ, we ensure that no other possible solution is removed [32]. The challenge here is that inequality (64) is non-convex. However, in mixed-integer programming, when the solution $\hat{x}$ is a set of binary variables, as in G&TEP, we can reformulate the no-good constraint to a linear form, and ϵ can be set to 1. Therefore, the no-good cut constraint for G&TEP to exclude the solution $\{\hat{x}_l, \hat{x}_g\}$ is expressed in (65).

$$\| x - \hat{x} \| \geq \epsilon \tag{64}$$

$$\sum_{l \in \mathcal{L}^+, \hat{x}_l = 0} x_l + \sum_{g \in G^+, \hat{x}_g = 0} x_g + \sum_{l \in \mathcal{L}^+, \hat{x}_l = 1} (1 - x_l) + \sum_{g \in G^+, \hat{x}_g = 1} (1 - x_g) \geq 1 \tag{65}$$

In this work, we introduced a novel application of no-good cuts to check the global optimality. After solving the LB and UB problems, the solution $\{\hat{x}_l, \hat{x}_g\}$ obtained

from the LB problem can be excluded from the problem region by adding the no-good cut constraint (65) to the LB problem to evaluate alternative solutions. Considering that the objective value obtained from the UB problem (AC-OPF problem) provides a valid upper bound for the AC-G&TEP problem, while the lower bound obtained from the LB model represents a valid lower bound, if the new lower bound obtained by resolving the LB problem within the excluded region, LB^*, exceeds the UB associated with $\{\hat{x}_l, \hat{x}_g\}$, it indicates that any solution in the residual region cannot be better than the excluded solution $\{\hat{x}_l, \hat{x}_g\}$. Therefore, $\{\hat{x}_l, \hat{x}_g\}$ is the global optimal solution to the problem, as no other feasible solution can provide a lower objective value, resulting in an optimality gap of zero.

Proposition 1. Let $\hat{x} \in \mathcal{F}$ be a feasible solution to the original optimization problem with objective value $\hat{z} = f(\hat{x})$, where $\mathcal{F}$ is the feasible region. Let $\mathcal{F}' := \mathcal{F} \setminus \{\hat{x}\}$ denote the feasible set after applying a no-good cut excluding $\hat{x}$. If the optimal value of the LB problem over $\mathcal{F}'$, denoted LB', satisfies $LB' > \hat{z}$, then $\hat{x}$ is the globally optimal solution to the original problem over $\mathcal{F}$.

Proof. Assume, for contradiction, that $\hat{x}$ is not globally optimal. Then, there must exist some other feasible solution $x' \in \mathcal{F}$, with objective value $f(x') < \hat{z}$. Since $\hat{x} \notin \mathcal{F}'$ but $x' \in \mathcal{F}'$, the LB problem solved over $\mathcal{F}'$ would have detected x' and returned a lower bound $LB' \leq f(x') < \hat{z}$, which contradicts the assumption that $LB' > \hat{z}$. Therefore, no such x' exists, and $\hat{x}$ is the globally optimal solution over $\mathcal{F}$. ■

3.4. Global-G&TEP algorithm

Algorithm 1 outlines the pseudocode for Global-G&TEP approach. The algorithm begins by setting solver parameters: RT for the tightness level of the proposed MISOCP relaxation ($RT = 0$ ignores relaxation-tightening constraints, $RT = 1$ applies these constraints to all existing lines, and $RT = 2$ extends them to candidate lines as well), gap^{tol} for the desired optimality gap, and np for the number of threads used for parallel computing. Additionally, there are two flags: G, which indicates the consideration of generation expansion, and the No-good-cut flag, which enables the no-good cut technique. These settings make the proposed approach quite flexible. The algorithm operates in a loop with two stopping criteria: a specified number of iterations (i.e., $i_{\max}$) or achieving the desired optimality gap (i.e., gap^{tol}).

Within the main loop, FBBT is first applied to tighten the variable bounds. Subsequently, the LB problem, which is a MISOCP relaxation, is solved to determine a candidate combination of lines and generating units ($\hat{x}_l$, $\hat{x}_g$) and establish a lower bound for the objective function (LB^{iter}). Then, the UB problem (AC-OPF problem) is solved for the given ($\hat{x}_l$, $\hat{x}_g$) to find a valid upper bound for the problem. If the

Algorithm 1 Proposed Global-G&TEP algorithm

Input system information
Set i_{max} and gap^{tol}
Set $G \leftarrow \{0, 1\}$ (default = 1)
Set $RT \leftarrow \{0, 1, 2\}$ (default = 0)
Set $np \leftarrow \{1, 2, ...\}$ (default = 1)
Set No-good-cut $\leftarrow$ {True, False} (default = True)
while $i \leq i_{max}$ **and** $gap \geq gap^{tol}$ **do**
  $bounds \leftarrow$ FBBT($bounds$)
  Run LB problem to find $LB^{iter}, \hat{x}_l, \hat{x}_g$
  $LB \leftarrow \max(LB, LB^{iter})$
  Run UB problem by fixing $\hat{x}_l, \hat{x}_g$
  $UB \leftarrow \max(UB, UB^{iter})$
  $gap \leftarrow (UB - LB)/UB$
  if $gap \leq gap^{tol}$ **then**
    break
  end if
  Run LB problem with no-good cuts to find LB^*
  if $LB^* \geq UB$ **then**
    $gap \leftarrow 0$ **and break**
  end if
  $bounds \leftarrow$ OBBT($bounds, UB$) (can be in parallel)
  if $i > i^{pre}$ **and** No changes in gap **then**
    if $RT \neq 2$ **then**
      $RT \leftarrow RT + 1$
    end if
  end if
end while
return x_l, x_g, gap

optimality gap between the obtained lower bound and upper bound falls below the desired optimality gap (gap^{tol}), the final solution is achieved. Otherwise, the no-good cut technique is applied. Incorporating the no-good cut into the LB problem ensures that the given solution is not revisited, allowing us to evaluate the new lower bound (LB^*) in the excluded feasible region. If LB^* exceeds the upper bound associated with solution ($\hat{x}_l$, $\hat{x}_g$), we can conclude that the solution ($\hat{x}_l$, $\hat{x}_g$) is the global optimal solution, achieving a zero optimality gap. Otherwise, OBBT is applied to further tighten the bounds of the decision variables. This results in tighter relaxations in the subsequent iteration due to the more stringent bounds. Furthermore, as mentioned earlier, OBBT is also applied to the binary variables to remove infeasible candidate lines and generating units, potentially decreasing search space and computational burden. Notably, both the LB and UB problems are initialized using standard warm-start values commonly employed in power system optimization. Specifically, voltage magnitudes are initialized at 1.0 per unit and voltage angles at zero, providing a numerically stable and physically meaningful starting point. The binary variables require no explicit initialization, as they are determined in the first iteration by solving the LB problem (MISOCP model).

The convergence of the proposed algorithm is guaranteed when a feasible solution exists. The solver automatically increases the relaxation-tightening level (RT) to further tighten the LB problem if the optimality gap does not improve after a predefined number of iterations i^{pre}. As a result, the LB problem becomes progressively tighter through the addition of relaxation-tightening constraints and finer piecewise approximations. This refinement ensures that the optimality gap between the LB and UB problems can be reduced below the desired threshold. If no feasible solution exists, the algorithm terminates after reaching the maximum number of iterations (i.e., $i_{\max}$). Notably, infeasibility in the UB problem (i.e., AC-OPF) indicates that the AC-G&TEP problem has no feasible solution under the current candidate configuration.

3.4.1. Computational complexity analysis

In this section, we analyze the theoretical complexity of each major component per iteration of the proposed Global-G&TEP algorithm using Big-O notation. First, FBBT, which propagates constraints via interval arithmetic, runs in $\mathcal{O}(E)$, where E is the number of constraint expressions, typically proportional to the number of continuous variables being tightened. FBBT operates independently of binary variables, and its cost is negligible relative to the core optimization tasks. Second, the LB problem, which is a MISOCP solved via a branch-and-bound strategy, has worst-case complexity $\mathcal{O}(2^B \cdot \text{poly}(C))$, where B and C represent the number of binary and continuous variables, respectively. Each node requires solving a convex

SOCP, typically handled by interior-point methods in CPLEX. The polynomial term poly(C) is usually approximated as C^3 for interior-point methods. Although the theoretical bound is exponential, solver-level features such as branching heuristics, cutting planes, presolve reductions, and parallel processing significantly improve performance in practice. The practical runtime using CPLEX scales approximately as $\mathcal{O}(B^k \cdot C^\alpha)$, where $k \in [1, 3]$ and $\alpha \in [2, 3]$, depending on problem sparsity, relaxation strength, and solver features. In typical instances, only a small fraction of the full branch-and-bound tree is explored, and interior-point solves at each node benefit from warm-starting and sparsity exploitation. Third, the UB problem is an NLP solved using IPOPT, with runtime approximately $\mathcal{O}(I \cdot C^\alpha)$, where I is the number of interior-point iterations and $\alpha \in [2, 3]$, depending on problem sparsity and structure. However, solving the AC-OPF model using IPOPT is generally very efficient and adds minimal overhead compared to the LB model.

When a no-good cut is triggered, it only requires an additional LB re-solve. Finally, OBBT solves up to $2P$ continuous relaxations to tighten bounds, where P is the number of variables being tightened, with worst-case complexity $\mathcal{O}(P \cdot C^3)$. This step is parallelized in practice to reduce wall-clock time. Notably, increasing RT from 0 to 1 adds continuous variables in proportion to the number of buses, existing lines, and piecewise segments, while RT = 2 introduces approximately 19 additional continuous variables per candidate line along with more binary variables. As the number of buses and candidate lines increases, higher RT levels significantly enlarge the problem size. For instance, in the 118-bus system, the number of continuous variables roughly triples when increasing RT from 0 to 1, which can affect the LB problem time in corresponding iterations.

4. Numerical results

4.1. Test systems

The proposed Global-G&TEP solver is evaluated on three widely-used AC transmission system test cases: the IEEE 24-bus system, the 46-bus Southern Brazilian system, and the IEEE 118-bus system. Additionally, to assess the scalability of the proposed method for real-world applications, it is tested on a recently developed large-scale Case1354pegase benchmark, which consists of 1354 buses [33].

4.1.1. Definition of candidate generating unit sets

Candidate generating unit sets are defined for the first three cases (i.e., 24-bus, 46-bus, and 118-bus systems). At each bus, we consider a standard generating unit with an active power generation range of 0 to 600 MW. The reactive power generation

for each unit is considered to range from -200 MVAr to 200 MVAr. The annualized investment costs for generating units over the planning horizon are randomly selected from a uniform distribution between $5 million and $15 million, using a uniform probability distribution. Data for candidate generating units for the 1354-bus system can be found in [33].

Table 1: Test system configuration and problem size for AC-G&TEP instances

Characteristics/Test systems	IEEE 24-bus	South Brazilian 46-bus	IEEE 118-bus	Case1354pegase
Existing lines	34	47	175	1991
Existing generating units	14	17	54	260
Candidate lines	41	79	30	30
Candidate generating units	24	46	118	50
Binary variables	65	125	148	80
Continuous variables	721	1238	2369	21537

Table 1 summarizes the characteristics of each test system, including the number of existing and candidate transmission lines, generating units, binary variables, and continuous variables. The Case1354pegase system features over 21,000 continuous variables and 80 binary variables, corresponding to the total number of candidate generating units and transmission lines.

The code is implemented in Julia 1.7.3 [34], utilizing the JuMP v0.21 [35] optimization modeling language. The LB models are solved using ILOG CPLEX 12.9 [36], while the UB model is solved using IPOPT version 3.12.10 [37]. Simulations are conducted on an ASUS PC with 8 GB of RAM and a 2.40 GHz Intel CPU. To benchmark the performance of general-purpose global MINLP solvers, SCIP 9.0.0 [38] and Couenne [39] are tested on a high-performance computing (HPC) platform featuring 40 Intel Skylake cores running at 2.1 GHz per node.

4.2. AC-TEP results

As no dedicated global optimization solver currently exists for the AC-G&TEP problem, we evaluate the performance of the proposed method by comparing its TEP variant with several advanced solvers. First, we consider two most

recent and advanced global AC-TEP solvers: the SOCP-based global solver enhanced with relaxation-tightening techniques proposed in [10], and the SDP-based branch-and-bound solver introduced in [9]. The best results in terms of optimality gap are considered from these solvers for comparison. Additionally, we compare our results with a recent AC-G&TEP optimization method proposed in [25], which solve AC-G&TEP locally using a metaheuristic-based approach using hybrid algorithms such as HBA-TS and DE-TS. Due to the unavailability of candidate generation unit data, the comparison is limited to the TEP results provided for the IEEE 24-bus system. Finally, general-purpose global MINLP solvers SCIP and Couenne are included as baselines to assess computational performance and optimality quality.. SCIP and Couenne are configured with their default settings. To isolate the TEP component in proposed Global-G&TEP, the G flag is set to zero. The numerical results for the IEEE 24-bus system, the 46-bus Southern Brazilian system, and the IEEE 118-bus system are shown in Tables 2-4.

Table 2: AC-TEP results for 24-bus test system

Solver	Objective value	Optimality gap (%)	Runtime (Sec.)
Global-G&TEP (RT = 0) (No-good-cut = True)	173.86	0.000	13.3
[10]	UB = 173.86 LB = 173.79	0.040	17.5
[9]	173.86	-	955
[25]	174.07	-	180
SCIP	UB = 173.86 LB = 173.86	0.000	2696 on HPC
Couenne	UB = - LB= 172.34	-	3600 on HPC

For all test systems, the proposed Global-G&TEP solver consistently outperforms existing global optimization approaches in both solution quality and computational efficiency. For instance, in the 46-bus system (Table 3), the global-TEP solver proposed in [10] achieves an optimality gap of 0.139% in 2513 seconds, whereas the proposed method obtains the same planning solution with a zero optimality gap in just 21 seconds. A similar pattern is observed for the 118-bus system (Table

Table 3: AC-TEP results for 46-bus test system

Solver	Objective value	Optimality gap (%)	Runtime (Sec.)
Global-G&TEP (RT = 0) (No-good-cut = True)	143.591	0.000	20.9
[10]	UB = 143.591 LB = 143.391	0.139	2513
SCIP	UB = 245.939 LB = 132.492	46.116	3H on HPC
Couenne	UB = - LB = 141.52615	-	3H on HPC

Table 4: AC-TEP results for 118-bus test system

Solver	Objective value	Optimality gap (%)	Runtime (Sec.)
Global-G&TEP (RT = 0) (No-good-cut = True)	51.706	0.000	27.1
[10]	UB = 51.706 LB = 51.694	0.022	726
SCIP	UB = - LB = 38.989	-	3H on HPC
Couenne	UB = - LB = 18.695	-	3H on HPC

4), where the proposed solver reaches the same optimal solution as in [10] while reducing runtime by approximately 96.3%. These results highlight the effectiveness and scalability of the proposed framework.

The comparison with the SDP-based solver in [9] for the 24-bus system shows that both SDP and SOCP relaxations achieve the same optimal solution, indicating that the SOCP-based relaxation when combined with bound tightening techniques, offers relaxation tightness comparable to that of SDP relaxations. However, as presented in Table 2, the SDP-based solver in [9] requires 955 seconds to converge, while the SOCP-based solvers in [10] and the proposed method reach the same planning solutions in just 17.5 and 13.3 seconds, respectively. This significant reduction in runtime demonstrates that SDP relaxations, despite their tightness, lack scalability due to their difficulty in integrating into mixed-integer frameworks and the need to solve many SDP subproblems across branch-and-bound nodes.

The comparison with the local AC-G&TEP solver introduced in [25] on the IEEE 24-bus system, as shown in Table 2, reveals that [25] yields a feasible solution with an objective value of 174.071, while the proposed Global-G&TEP method achieves a superior objective value of 173.86. Although both solutions are feasible, the discrepancy confirms that the local solver may converge to a suboptimal solution, highlighting the need for globally optimal approaches when addressing highly non-convex planning problems.

Lastly, the performance of general-purpose global MINLP solvers, SCIP and Couenne, highlights their limitations in addressing non-convex AC-based planning problems. While SCIP is able to solve the 24-bus case with a zero optimality gap, it requires 2860 seconds on a HPC node. As system size increases, both solvers exhibit significant performance degradation. For the 46-bus system, SCIP achieves an optimality gap exceeding 46% after three hours, whereas Couenne fails to identify any feasible solution. In the 118-bus system, neither solver returns an upper bound, and the reported lower bounds are notably weak, underscoring their inability to scale with problem size.

4.3. AC-G&TEP results

The coordinated AC-G&TEP problem is considered in this section. By setting flag $G = 1$ the proposed Global-G&TEP framework solves the coordinated planning problem with a guaranteed optimality gap. The performance of the Global-G&TEP solver is benchmarked against two state-of-the-art global MINLP solvers, SCIP and Couenne. Simulation results for the four aforementioned test systems are presented in Tables 5–8.

As illustrated by the results from Tables 5-7, enabling relaxation-tightening

Table 5: AC-G&TEP results for 24-bus test system

Solver	Objective value	Optimality gap (%)	Runtime (Sec.)
Global-G&TEP (RT = 0) (No-good-cut = False)	UB = 54.46 LB = 54.45	0.025	5.9
Global-G&TEP (RT = 2) (No-good-cut = False)	UB = 54.46 LB =54.45	0.023	18.1
Global-G&TEP (RT = 0) (No-good-cut = True)	54.46	0.000	8.1
SCIP	UB = 54.46 LB = 53.39	1.965	2860 on HPC
Couenne	UB = - LB = 53.22	-	3000 on HPC

Table 6: AC-G&TEP results for 46-bus test system

Solver	Objective value	Optimality gap (%)	Runtime (Sec.)
Global-G&TEP (RT = 0) (No-good-cut = False)	UB = 109.82 LB = 109.52	0.275	12.5
Global-G&TEP (RT = 2) (No-good-cut = False)	UB = 109.82 LB = 109.59	0.209	237.2
Global-G&TEP (RT = 0) (No-good-cut = True)	109.82	0.000	23.6
SCIP	UB = 264.4 LB = 108.2	144.41	10H on HPC
Couenne	UB= - LB = 73.25	-	10H on HPC

Table 7: AC-G&TEP results for 118-bus test system

Solver	Objective value	Optimality gap (%)	Runtime (Sec.)
Global-G&TEP (RT = 0) (No-good-cut = False)	UB = 51.42 LB = 51.41	0.020	23.1
Global-G&TEP (RT = 2) (No-good-cut = False)	UB = 51.42 LB = 51.41	0.014	404.8
Global-G&TEP (RT = 0) (No-good-cut = True)	51.42	0.000	41.3
Global-G&TEP (RT = 0) (with OBBT)	UB = 51.42 LB = 51.41	0.016	321.5
SCIP	UB = - LB=42.02	-	18H on HPC
Couenne	UB = 51.77 LB=19.40	62.524	18H on HPC

Table 8: AC-G&TEP results for 1354-bus test system

Solver	Objective value	Optimality gap (%)	Runtime (Sec.)
Global-G&TEP (RT = 0) (No-good-cut = False)	UB = 81560.1 LB = 81498.3	0.076	8H,45min
SCIP	-	-	24H on HPC
Couenne	UB = - LB = 23329.6	-	24H on HPC

constraints ($RT = 2$) improves the optimality gap compared to when these constraints are disabled ($RT = 0$). With $RT = 2$, the relaxation-tightening constraints strengthen the relaxation in the LB problem, leading to an improved lower bound. However, this improvement enlarges the problem size and complexity by introducing more constraints and variables, and comes at the cost of a significantly increased runtime. Notably, increasing RT from 0 to 2 results in a threefold increase in runtime for the 24-bus case and an 18-fold increase for the 46-bus case, illustrating the exponential growth in computational time with increasing system size.

The novel application of the no-good cut technique significantly improves solution quality while reducing the runtime required to achieve global optimality. For instance, as shown in Table 7, for the 118-bus system, the proposed solver achieves a zero optimality gap in just 41.3 seconds with the no-good cut technique, whereas without it, the solver requires 404.8 seconds to reach a 0.014% gap at $RT = 2$. Incorporating no-good cuts allows the algorithm to bypass the computationally expensive relaxation-tightening constraints and avoid multiple iterations by enabling the possibility of certifying global optimality early. Notably, as shown in Tables 5–7, the effectiveness of the no-good cut technique is maintained as system size increases. From the 24-bus to the 118-bus case, the number of decision variables more than triples, yet the solver continues to certify global optimality efficiently with minimal additional runtime. These results demonstrate that the proposed no-good cut technique is tailored for the AC-G&TEP problem and contributes to the solver's efficiency and scalability.

The impact of the proposed OBBT is evaluated in the 118-bus system, as presented in Table 7. Applying the proposed OBBT improves the optimality gap by providing a stronger relaxation of the lower-bound problem, which is directly related to the tightness of the variable bounds. The proposed OBBT utilizes the continuous relaxed version of the problem, resulting in a short runtime. Additionally, since the proposed solver enables parallel computing, solving OBBT in parallel can further reduce the total runtime.

To further evaluate the scalability of the solver, we tested the performance of the proposed approach on the large-scale 1354-bus system, which includes 21537 continuous variables and 80 binary variables. As illustrated in Table 8, the Global-G&TEP solver is able to find a solution with an optimality gap of 0.076% in 8 hours and 45 minutes. Given that G&TEP typically considers a long-term planning horizon of 15 to 20 years, the observed runtime is acceptable for practical applications and highlights the method's scalability for large-scale power system planning.

The results from global MINLP solvers, Couenne and SCIP, demonstrate their limitations in solving the AC-G&TEP problem. SCIP is able to return a solution

only for the small 24-bus case, requiring 2,860 seconds to achieve a 1.965% optimality gap. However, as the test system size increases, SCIP fails to converge, even after extended runtimes (e.g., 24 hours for the 1354-bus system). Similarly, Couenne fails to produce feasible solutions or achieve convergence for any of the test cases, even after extended runtimes, and its lower bounds degrade significantly as the problem size increases. This is due to the lack of problem-specific structure in these general-purpose solvers, which limits their ability to generate tight relaxations and leads to excessive exploration of infeasible or suboptimal regions of the solution space. These results highlight the necessity for a specialized global solver for the AC-G&TEP problem, capable of providing global optimal planning decisions within reasonable computational times.

Comparing the results for AC-TEP and AC-G&TEP, we observe that solving the joint G&TEP problem may increase the computational time due to the increased number of binary variables and the overall larger problem size. However, solving the joint G&TEP problem results more optimal than the best one obtained from the TEP problem. For instance, in the 46-bus system, the objective value decreases from \$143.591 million to \$109.82 million when solving the coordinated G&TEP problem compared to solving the TEP alone. This reduction can be attributed to the interdependencies between planning systems, which make separate planning approaches suboptimal. These findings suggest the superiority of the co-optimization G&TEP to have more cost-effective solutions.

Lastly, to emphasize the importance of a global optimization framework for the AC-G&TEP problem, we compare the total objective values obtained using the proposed Global-G&TEP solver and the state-of-the-art local MINLP solver Knitro [40]. All solver settings are kept at their default values, except for the maximum number of mixed-integer heuristic iterations, which is increased to 10,000 (i.e., *mip_heuristic_maxit = 10000*) to allow sufficient time for exploring the solution space and identifying high-quality local solutions. As illustrated in Figure 2, for the small-scale 24-bus system, both solvers converge to the same solution. However, for the larger 46-bus and 118-bus systems, Knitro consistently converges to feasible yet suboptimal solutions, yielding higher objective values compared to the globally optimal solutions obtained by the proposed Global-G&TEP solver. Similarly, for the 1354-bus test system, Knitro yields an objective of 81626.7, while the Global-G&TEP method attains a superior value of 81560.1. These results highlight the necessity of global optimization frameworks for solving the non-convex AC-G&TEP problem.

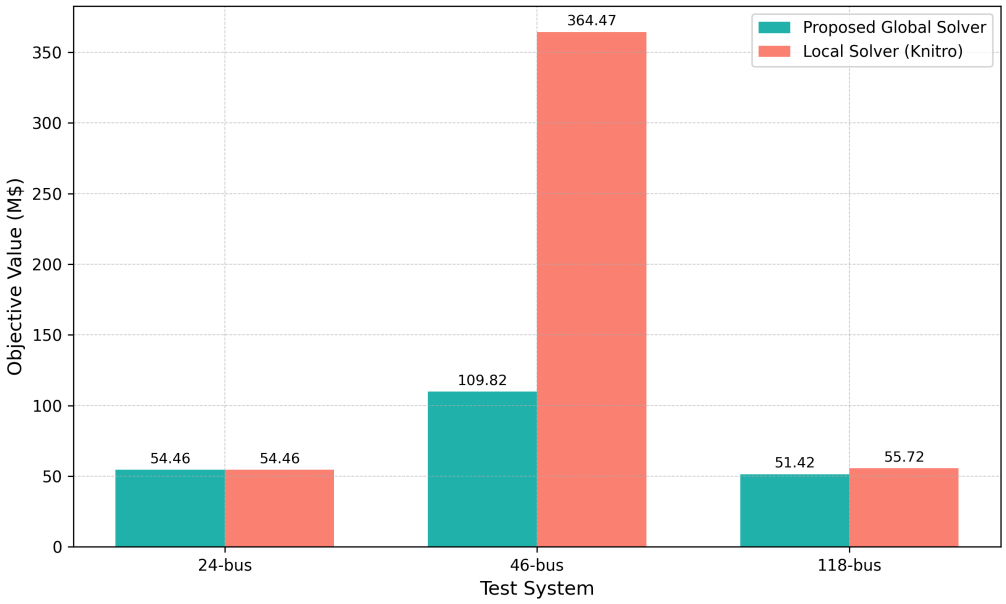

Figure 2: Objective value comparison between the proposed Global-G&TEP and a local Knitro solver across the 24-, 46-, and 118-bus systems.

5. Conclusion

This study proposes a global approach for co-optimizing G&TEP, incorporating compensator expansion planning. The G&TEP problem, modeled as an MINLP using AC network representation, is addressed through a framework based on SOCP relaxations, which can be further tightened using relaxation-tightening constraints. Two bound-tightening techniques, FBBT and OBBT, are integrated to significantly tighten the bounds of decision variables, resulting in stronger relaxations and faster convergence. Additionally, a novel application of no-good cut constraints is introduced, enabling the solver to explore alternative feasible regions effectively.

Comparative analyses are conducted for both TEP and G&TEP versions of the solver. The TEP version, benchmarked against existing global solvers for AC-TEP, demonstrates superior performance by obtaining higher-quality solutions faster. The G&TEP version is evaluated against state-of-the-art global MINLP solvers, SCIP and Couenne, which are shown to be incapable of solving the AC-G&TEP efficiently. In contrast, the proposed method finds an optimal solution within a reasonable timeframe. For instance, the solver achieves the optimal solution for the 118-bus system in 41 seconds, whereas SCIP and Couenne fail to converge after 13 hours. Furthermore, coordinated planning is observed to yield lower total costs compared

to solving the problems independently. The proposed approach is further validated on the large-scale 1354-bus system, demonstrating its scalability. These results underscore its potential for future studies addressing stochastic uncertainties inherent in renewable energy sources.

Future research can extend the proposed framework to account for uncertainty associated with long-term demand forecasts and, in particular, the inherent variability of renewable energy sources. Additionally, incorporating dynamic aspects, such as multi-period planning and generator ramping constraints, would also improve applicability in systems with high renewable energy penetration.

CRediT authorship contribution statement

Ghazaleh Mozafari: Writing – original draft, Writing – review & editing, Coding, Software, Methodology, Formal analysis. **Mahdi Mehrtash**: Conceptualization, Methodology, Coding, Formal analysis, Writing – Review & editing. **Yankai Cao**: Conceptualization, Writing – Review & editing, Supervision, Funding acquisition. **Bhushan Gopaluni**: Writing – Review & editing, Supervision.

Acknowledgment

Mahdi Mehrtash is partially supported by the Ralph O'Connor Sustainable Energy Institute (ROSEI), based in Johns Hopkins University's Whiting School of Engineering, in the framework of Spark Awards.

Appendix

References

[1] A. Conejo, L. Baringo, J. Kazempour, A. Siddiqui, Investment in Electricity Generation and Transmission, Springer Int. Publ., Cham, Switzerland, 2016. doi:10.1007/978-3-319-29501-5.

[2] A. Rose, I. Perez-Arriaga, Regional trade and expansion planning (rtep) model: Model for regional power sector integration in africa, Renew. Energy Focus 42 (2022) 101–114. doi:10.1016/j.ref.2022.05.003.

[3] S. Goodarzi, M. Gitizadeh, A. Abbasi, An efficient linear network model for transmission expansion planning based on piecewise mccormick relaxation, IET Gener. Transm. Distrib. 13 (2019) 5404–5412. doi:10.1049/iet-gtd.2019.0878.

[4] N. Alguacil, A. L. Motto, A. J. Conejo, Transmission expansion planning: A mixed-integer LP approach, IEEE Trans. Power Syst. 18 (3) (2003) 1070–1077. doi:10.1109/TPWRS.2003.814891.

[5] M. A. El-Meligy, A. M. El-Sherbeeny, Hybrid robust/stochastic transmission expansion planning considering uncertainties in generators' offer prices: A second-order cone program approach, Electr. Power Syst. Res. 203 (2022) 107631. doi:10.1016/j.epsr.2021.107631.

[6] H. Zhang, G. T. Heydt, V. Vittal, J. Quintero, An improved network model for transmission expansion planning considering reactive power and network losses, IEEE Trans. Power Syst. 28 (3) (2013) 3471–3479. doi:10.1109/TPWRS.2013.2250318.

[7] Z.-Y. Wang, H.-D. Chiang, On the feasibility of AC and DC optimal power flow models: Analytics and comparison, in: Proceedings of the IEEE Power and Energy Society General Meeting (PESGM), 2021, pp. 1–5. doi:10.1109/PESGM46819.2021.9638005.

[8] J. A. Taylor, F. S. Hover, Conic AC transmission system planning, IEEE Trans. Power Syst. 28 (2) (2013) 952–959. doi:10.1109/TPWRS.2012.2214490.

[9] B. Ghaddar, R. A. Jabr, Power transmission network expansion planning: A semidefinite programming branch-and-bound approach, Eur. J. Oper. Res. 274 (3) (2019) 837–844. doi:10.1016/j.ejor.2018.10.035.

[10] M. Mehrtash, Y. Cao, A new global solver for transmission expansion planning with AC network model, IEEE Trans. Power Syst. 37 (1) (2022) 282–293. doi:10.1109/TPWRS.2021.3086085.

[11] C. Antunes, A. Martins, I. Brito, A multiple objective mixed integer linear programming model for power generation expansion planning, Energy 29 (4) (2004) 613–627. doi:10.1016/j.energy.2003.10.012.

[12] J. Hu, X. Xu, H. Ma, Z. Yan, Distributionally robust co-optimization of transmission network expansion planning and penetration level of renewable generation, Journal of Modern Power Systems and Clean Energy 10 (3) (2022) 577–587. doi:10.35833/MPCE.2020.000744.

[13] M. Mehrtash, B. F. Hobbs, R. Mahroo, Necessity of joint resource and transmission expansion planning in presence of system and policy uncertainties,

in: Proceedings of the IEEE Texas Power and Energy Conference (TPEC), 2023, pp. 1–6. doi:10.1109/TPEC56611.2023.10078637.

[14] M. Taherkhani, S. H. Hosseini, M. S. Javadi, J. P. Catalão, Scenario-based probabilistic multi-stage optimization for transmission expansion planning incorporating wind generation integration, Electr. Power Syst. Res. 189 (2020) 106601. doi:10.1016/j.epsr.2020.106601.

[15] C. Li, A. J. Conejo, P. Liu, B. P. Omell, J. D. Siirola, I. E. Grossmann, Mixed-integer linear programming models and algorithms for generation and transmission expansion planning of power systems, Eur. J. Oper. Res. 297 (3) (2022) 1071–1082. doi:10.1016/j.ejor.2021.06.024.

[16] J. Aghaei, N. Amjady, A. Baharvandi, M. A. Akbari, Generation and transmission expansion planning: MILP–based probabilistic model, IEEE Trans. Power Syst. 29 (4) (2014) 1592–1601. doi:10.1109/TPWRS.2013.2296352.

[17] F. A. Bukhari, K. A. Alnowibet, Integrated robust generation and transmission network expansion planning considering time duration uncertainty, Electr. Power Syst. Res. 239 (2025) 111269. doi:10.1016/j.epsr.2024.111269.

[18] M. Mehrtash, B. F. Hobbs, R. Mahroo, Y. Cao, Does choice of power flow representation matter in transmission expansion optimization? A quantitative comparison for a large-scale test system, IEEE Trans. Ind. Appl. 60 (1) (2024) 1433–1441. doi:10.1109/TIA.2023.3317228.

[19] M. Ansari, S. Pirouzi, M. Kazemi, A. Naderipour, M. Benbouzid, Renewable generation and transmission expansion planning coordination with energy storage system: A flexibility point of view, Appl. Sci. 11 (8) (2021) 3303. doi:10.3390/app11083303.

[20] C. Roldán, A. S. de la Nieta, R. García-Bertrand, R. Mínguez, Robust dynamic transmission and renewable generation expansion planning: Walking towards sustainable systems, Int. J. Electr. Power Energy Syst. 96 (2018) 52–63. doi:10.1016/j.ijepes.2017.09.021.

[21] Y. Tohidi, L. Olmos, M. Rivier, M. R. Hesamzadeh, Coordination of generation and transmission development through generation transmission charges—a game theoretical approach, IEEE Trans. Power Syst. 32 (2) (2017) 1103–1114. doi:10.1109/TPWRS.2016.2581218.

[22] A. Davoodi, A. Reza Abbasi, S. Nejatian, Multi-objective dynamic generation and transmission expansion planning considering capacitor bank allocation and demand response program constrained to flexible-securable clean energy, Sustain. Energy Technol. Assess. 47 (2021) 101469. doi:10.1016/j.seta.2021.101469.

[23] M. Mahdavi, M. S. Javadi, J. P. S. Catalão, Integrated generation-transmission expansion planning considering power system reliability and optimal maintenance activities, Int. J. Electr. Power Energy Syst. 145 (2023) 108688. doi:10.1016/j.ijepes.2022.108688.

[24] F. Dehghani, M. A. Shafiyi, Integration of hybrid renewable energy sources with the power system considering their economic complementarity, IET Renew. Power Gener. 17 (15) (2023) 3638–3650. doi:10.1049/rpg2.12871.

[25] J. E. Chillogalli, S. P. Torres, R. A. Romero, W. E. Chumbi, F. Astudillo-Salinas, D. Ochoa-Correa, Co-optimization of generation and ac transmission networks, considering reactive power allocation and network power losses, IEEE Access 12 (2024) 116428–116441. doi:10.1109/ACCESS.2024.3446239.

[26] M. Mehrtash, A. Kargarian, Risk-based dynamic generation and transmission expansion planning with propagating effects of contingencies, Int. J. Electr. Power Energy Syst. 118 (2020) 105762. doi:10.1016/j.ijepes.2019.105762.

[27] R. A. Jabr, Optimization of reactive power expansion planning, Electr. Power Compon. Syst. 39 (12) (2011) 1285–1301. doi:10.1080/15325008.2011.567220.

[28] X. Yin, H. Chen, Z. Liang, Q. He, Robust transmission expansion planning using pair-based convex hull uncertainty sets under high penetration of renewable energy generation, Energy Rep. 8 (2022) 4491–4501. doi:10.1016/j.egyr.2022.03.084.

[29] H. L. Hijazi, C. J. Coffrin, P. V. Hentenryck, Convex quadratic relaxations for mixed-integer nonlinear programs in power systems, Math. Program. Comput. 9 (3) (2017) 321–367. doi:10.1007/s12532-016-0112-z.

[30] P. Belotti, S. Cafieri, J. Lee, L. Liberti, On feasibility based bounds tightening, [Online]. Available: https://hal-enac.archives-ouvertes.fr/hal-00935464 (2012).

[31] G. Ceyhan, M. Köksalan, B. Lokman, Extensions for benders cuts and new valid inequalities for solving the european day-ahead electricity market clearing problem efficiently, Eur. J. Oper. Res. 300 (2) (2022) 713–726. doi:10.1016/j.ejor.2021.10.007.

[32] C. D'Ambrosio, A. Frangioni, L. Liberti, A. Lodi, On interval-subgradient and no-good cuts, Oper. Res. Lett. 38 (5) (2010) 341–345. doi:10.1016/j.orl.2010.05.010.

[33] M. Mehrtash, B. F. Hobbs, Y. Cao, A large-scale test system for transmission expansion planning with AC networks model, in: Proceedings of the IEEE Texas Power and Energy Conference (TPEC), 2022, pp. 1–5. doi:10.1109/TPEC54980.2022.9750848.

[34] J. Bezanson, A. Edelman, S. Karpinski, V. B. Shah, Julia: A fresh approach to numerical computing, SIAM Rev. 59 (1) (2017) 65–98. doi:10.1137/141000671.

[35] M. Lubin, O. Dowson, J. D. Garcia, et al., Jump 1.0: Recent improvements to a modeling language for mathematical optimization, Math. Program. Comput. 15 (2023) 581–589. doi:10.1007/s12532-023-00239-3.

[36] IBM Corporation, IBM ILOG CPLEX Optimization Studio V12.1: User's Manual, IBM, [Online]. Available: https://www.ibm.com/products/ilog-cplex-optimization-studio (2009).

[37] A. Wächter, L. Biegler, On the implementation of an interior-point filter line-search algorithm for large-scale nonlinear programming, Math. Program. 106 (2006) 25–57. doi:10.1007/s10107-004-0559-y.

[38] T. Achterberg, SCIP: Solving constraint integer programs, Math. Program. Comput. 1 (1) (2009) 1–41. doi:10.1007/s12532-008-0001-1.

[39] P. Belotti, J. Lee, L. Liberti, F. Margot, A. Wächter, Branching and bounds tightening techniques for non-convex MINLP, Optim. Methods Softw. 24 (4-5) (2009) 597–634. doi:10.1080/10556780903087124.

[40] Artelys Knitro, Knitro solver, [Online]. Available: https://www.artelys.com/solvers/knitro/ (Feb. 2025).